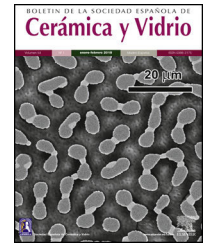




BOLETIN DE LA SOCIEDAD ESPAÑOLA DE  
**Cerámica y Vidrio**

[www.elsevier.es/bsecv](http://www.elsevier.es/bsecv)



# Evaluation of the photocatalytic activity of ZnO nanorods and nanoflowers grown from seed layers deposited by spin coating

Antonia del Rocío López Guemez<sup>a</sup>, Adrián Cordero García<sup>a</sup>, José Luis Cervantes López<sup>b</sup>, Hermicenda Pérez Vidal<sup>a</sup>, Laura Lorena Díaz Flores<sup>b,\*</sup>

<sup>a</sup> División Académica de Ciencias Básicas, Universidad Juárez Autónoma de Tabasco, Villahermosa, Tabasco, Mexico

<sup>b</sup> División Académica de Ingeniería y Arquitectura, Universidad Juárez Autónoma de Tabasco, Villahermosa, Tabasco, Mexico

## ARTICLE INFO

### Article history:

Received 20 March 2023

Accepted 19 June 2023

Available online 5 July 2023

### Keywords:

Zinc oxide

Sol-gel

Hydrothermal growth

Nanostructures

Photocatalysis

## ABSTRACT

The increase in pollution, using photocatalytic materials to degrade organic pollutants remains in force. ZnO is the most used semiconductors for photocatalytic applications. The oriented growth of nanostructures on substrates or seed layers (SL) improves the physical and chemical properties compared to the bulk-grown material. In this work, the photocatalytic efficiency of ZnO nanorods and nanoflowers was evaluated, obtained by hydrothermal growth (HG) over SL deposited by the spin-coating technique (SCT). The characterizations results showed two types of growth: 1D nanostructures with a dimension in the range of 400–1000 nm and diameters of 70–100 nm, and 1D microstructures with approximate 5–11 μm length and diameters of 1–2 μm. However, in the 7 SL system, micro prisms were generated, which led to the formation of 3D nanostructures (micro flowers) of ZnO with a maximum of 6 μm in diameter. The system with 1D and 3D ZnO nanostructures, grown in 7 SL, was the most efficient methylene blue degradation. Achieving 100% transformation in 120 min, with a rate constant of  $2.98 \times 10^{-2} \text{ min}^{-1}$ . The results show that the SCT deposit combined with the sol-gel method and HG produces 1D and 3D structures with high potential in photocatalytic degradation.

© 2023 The Authors. Published by Elsevier España, S.L.U. on behalf of SECV. This is an open access article under the CC BY-NC-ND license (<http://creativecommons.org/licenses/by-nc-nd/4.0/>).

\* Corresponding author.

E-mail address: [laura.diaz@ujat.mx](mailto:laura.diaz@ujat.mx) (L.L. Díaz Flores).

<https://doi.org/10.1016/j.bsecv.2023.06.003>

0366-3175/© 2023 The Authors. Published by Elsevier España, S.L.U. on behalf of SECV. This is an open access article under the CC BY-NC-ND license (<http://creativecommons.org/licenses/by-nc-nd/4.0/>).

## Evaluación de la actividad fotocatalítica de nanovarillas y nanoflores de ZnO crecidas a partir de capas semillas depositadas por spin coating

### R E S U M E N

#### Palabras clave:

Óxido de zinc

Sol-gel

Crecimiento hidrotérmico

Nanoestructuras

Fotocatálisis

El aumento de la contaminación, el empleo de materiales fotocatalíticos para degradar contaminantes orgánicos continúa vigente. El óxido de zinc (ZnO) es el semiconductor más utilizado para aplicaciones fotocatalíticas. El crecimiento orientado de nanoestructuras sobre capas semillas (SL) mejora las propiedades físicas y químicas comparado con el material crecido en bulto. En este trabajo se evaluó la eficiencia fotocatalítica de nanovarillas y nanoflores de ZnO obtenidas por crecimiento hidrotérmico (HG) sobre SL depositadas por la técnica *spin coating* (SCT). Los resultados de las caracterizaciones mostraron dos tipos de crecimiento: nanoestructuras 1D con dimensiones en el rango de 400 a 1.000 nm y diámetros de 70 a 100 nm, y microestructuras 1D con longitud aproximada de 5 a 11  $\mu\text{m}$  y diámetros de 1 a 2  $\mu\text{m}$ . Sin embargo, en el sistema de 7 SL se generaron micropismas orientados, generando nanoestructuras 3D (microflores) con un diámetro máximo de 6  $\mu\text{m}$ . Este sistema fue el más eficiente en la degradación de azul de metileno. Degradando de 100% en 120 min, con una constante de velocidad de  $2,98 \times 10^{-2} \text{ min}^{-1}$ . Los resultados indican que la SCT combinada con el método sol-gel y el HG produce estructuras 1D y 3D con alto potencial de degradación fotocatalítica.

© 2023 Los Autores. Publicado por Elsevier España, S.L.U. en nombre de SECV. Este es un artículo Open Access bajo la licencia CC BY-NC-ND (<http://creativecommons.org/licenses/by-nc-nd/4.0/>).

## Introduction

ZnO is used as a sunscreen and in solar cells due to its optoelectronic properties, making it a material of interest in research focused on solving water pollution problems. It has a forbidden band gap ( $\approx 3.2 \text{ eV}$ ) that makes it photosensitive to UV radiation, which allows the mobility of charge carriers ( $e^-/h^+$ ) on its surface, that produce redox reactions during the photocatalytic process [1]. In 1D nanostructures, the photocatalytic efficiency of ZnO is highly dependent on the polar planes, as they influence surface defects that affect adsorption and surface reactivity [2,3]. In the ZnO hexagonal wurtzite crystalline form, anisotropic crystal growth has been reported, with 1D nanostructures in the form of nanotubes, nanowires, nanofibers, and nanoneedles [4,5]. To obtain the 1D nanostructures, different methods have been used to deposit the SL, some of them are: pulsed laser deposition [6], spray pyrolysis [7], magnetron sputtering [8], electrodeposition and atomic layer deposition [9].

In relation to the use of ZnO 1D as a photocatalyst, the literature reports several studies in which this nanostructure has been synthesized from SL. In one of them SL were obtained from the atomic layer deposition method [10], to degrade methylene blue (MB). In this study, SL were deposited on silicon substrates with different thicknesses; they obtained long and dense nanorods arrays. In particular, the ZnO film with a thickness of 3 nm promoted the growth of dense and c-axis oriented ZnO nanorods arrays, which improved the photocatalytic efficiency for MB dye degradation under UV light irradiation, achieving 70% transformation after 4 h. In another study [11], the photocatalytic activity of ZnO nanorods was optimized. The nanorods were obtained by deposition of a ZnO SL using ultrasonic spray pyrolysis (USP) as the

deposition technique, followed by HG. ZnO nanorods were used as a photocatalyst to degrade an aqueous methylene blue (MB) solution, using UV light as an irradiation source. They report that the higher photocatalytic efficiency (83%) is related to the orientation of the dominant face surface in the (002) plane of ZnO in its wurtzite crystalline form since the exposure of the (002) plane facilitates the adsorption of  $\text{OH}^-$  ions, so the reaction between the interstitial oxygen holes with  $\text{OH}^-$  ions, increase the photocatalytic efficiency. In addition, the positive Zn-terminated faces (002) can easily adsorb the negatively charged MB molecules. In another research Bourfaa et al. obtained ZnO thin films with 200 nm thickness, using the RF sputtering method; to be used as SL to grow 1D ZnO structures, using the HG. As a result of the growth, they obtained nanorods with shapes in nanoflowers when the films were placed horizontally to the solution at the HG stage. The results of the photocatalytic degradation of MB showed that the nanorods degraded more than 65%, while the nanoflowers degraded more than 80%. This demonstrated that ZnO nanoflowers have a high-efficiency photodegradation, attributed to the photogenerated carriers in the band gap of ZnO structure [12]. In this context, the aforementioned work demonstrates that the SL deposition technique influences the ZnO particle size, orientation, density, and variation of the size and shapes of grown nanostructures. All of which influence the mechanism and photocatalytic activity.

Regarding that with combined use of SCT for the deposition of ZnO SL and subsequent HG, is possible to obtain vertically aligned 1D ZnO structures, with high density and thickness in the range of micrometers to nanometers, and these nanoforms have been used in solar cells, gas sensors, biomedical applications, field effect transistors, among others [13,14]. However, its potential in photocatalysis has not been evaluated to date. Therefore, in this research work, the

hydrothermal growth of 1D (nanorods) and 3D (microflowers) ZnO nanostructures was carried out from ZnO SL deposited in 3, 5 and 7 layers using SCT, for the photocatalytic degradation of MB.

## Experimental details

### Materials and reagents

For the synthesis of ZnO, the reagents used were zinc acetate dihydrate (Zn (CH<sub>3</sub>COO)<sub>2</sub>·2H<sub>2</sub>O, 99%) and 2-propanol (C<sub>3</sub>H<sub>8</sub>O, 99.5%) from J.T. Baker. Monoethanolamine (C<sub>2</sub>H<sub>7</sub>NO, 99%), hexamethylenetetramine (C<sub>6</sub>H<sub>12</sub>N<sub>4</sub>, 99%), Meyer. Methylene blue (C<sub>16</sub>H<sub>18</sub>N<sub>3</sub>SCl·3H<sub>2</sub>O, 98.5%) from Civeq. All reagents are used as they come in their trademark.

### Preparation of ZnO seed layers

A precursor solution (0.28 M) was obtained using the sol–gel method: first, 3.10 g of zinc acetate dihydrate was dissolved in 2-propanol, this solution was constantly stirred for 15 min. Then, 0.85 mL of monoethanolamine was added drop by drop. The mixture thus prepared was heated to 60 °C in a reflux system with constant stirring for 1 h. After this, the solution was laid down for 72 h at room temperature. Before the deposit of the ZnO films, glass substrates were washed for 10 min with a 2:1 solution of H<sub>2</sub>SO<sub>4</sub>:H<sub>2</sub>O<sub>2</sub>. Finally, 100 μL of the ZnO precursor solution (0.28 M) was deposited on a 2.5 cm<sup>2</sup> glass substrate, using the SCT to a speed of 3000 rpm for 30 s in a spin coating equipment model WS-400BZ6NPP/LITE. Between each layer of ZnO deposited, a drying stage was carried out for 1 h at 80 °C to evaporate the solvent and the remaining organic residues. The procedure for depositing the layers was repeated 3, 5, and 7 times depending on the obtained system. Then, ZnO coatings were placed in a muffle and calcined for 1 h at 500 °C. The ZnO coatings obtained were identified as S1-3L, S2-5L, and S3-7L, where S corresponds to the system and L to the deposited coating layers.

### Hydrothermal growth of ZnO nanostructures

For the growth of the ZnO nanorods, an equimolar solution (0.01 M) of zinc acetate dihydrate and hexamethylenetetramine was dissolved in distilled water and stirred for 30 min. Then, in an autoclave reactor BAOSHISHAN of 100 mL with Teflon container, the SL S1-3L added, S2-5L and S3-7L, and 25 mL of the AcZnD/HMTA solution, was heated in an oven for 3 h at 90 °C. After this time, the hydrothermal reactor was allowed to cool to room temperature. Finally, the ZnO nanostructure was water-washed distilled and dried for 10 min at 90 °C. The ZnO nanostructures thus obtained were identified as HG-S1-3L, HG-S2-5L, and HG-S3-7L where HG corresponds to hydrothermal growth, S corresponds to the system and L to the number of layers of the coating.

### Characterization of ZnO coatings

To determine the crystalline structure of the ZnO coatings, an Empyrean model Malvern Panalytical X-ray diffractometer

was used with Cu Kα<sub>1</sub> radiation (1.5406 Å), a step time of 0.404 s and a scanning angle of 2θ between 20° and 70°. Diffraction peaks were identified using ICDD file 01-079-9878. The surface morphology of the ZnO nanostructures and the thickness of the cross-sectional surfaces of the ZnO coatings were examined by a Tescan model Mira 3 scanning electron microscope (SEM), coupled with energy dispersive spectroscopy (EDS) Bruker model XFlash 6160. Force microscopy atomic (AFM) was developed using Witec ALPHA 300 equipment. Diffuse reflectance spectra of the HG were recorded using a Varian Cary 100 UV–Vis spectrophotometer equipped with an integration sphere of diffuse reflectance for solids.

### Evaluation of photocatalytic degradation

The photocatalytic activity of ZnO coatings (HG-S1-3L, HG-S2-5L, and HG-S3-7L) was evaluated in the degradation of 1 mgL<sup>-1</sup> of MB contaminant in an aqueous medium using λ = 254 nm UV light as activation source. Inside the Vidren brand photocatalytic reactor, was placed the dye solution, and six ZnO coatings (6.25 cm<sup>2</sup> area) with 3, 5, or 7 layers depending on the evaluated system. Prior to the start of irradiation to the photocatalytic system, the aqueous solution was continuously stirred in the dark for 30 min to ensure the adsorption/desorption equilibrium of the dye molecules on the surface of the ZnO nanostructures. Afterwards, the photocatalytic system was irradiated with UV light for 240 min, and took samples every 30 min. The MB transformation evolution, was followed with a Shimadzu TOC-VSCH brand total organic carbon (TOC) analyzer and Eq. (1):

$$\% \text{TOC} = \frac{\text{TOC}_0 - \text{TOC}_f}{\text{TOC}_0} \times 100 \quad (1)$$

where TOC<sub>0</sub> is the mineralization at time zero and TOC<sub>f</sub> is the final mineralization of each sample. The photodegradation reaction rate was calculated from the linear graph of ln(C<sub>0</sub>/C) against irradiation time (where C<sub>0</sub> is the initial MB concentration, C is the MB concentration at time t).

## Results and discussion

### Structural analysis

Fig. 1 shows the X-ray diffraction (XRD) the layer systems seeds (S1-3L, S2-5L and S3-7L) and hydrothermal growth (HG-S1-3L, HG-S2-5L and HG-S3-7L). All samples exhibit diffraction peaks in the (100), (002), (101), (102), (110), (103), and (200) at 2θ = 31.757°, 34.440°, 36.248°, 47.545°, 56.573°, 62.876° and 66.350° respectively, which correspond to the hexagonal wurtzite structure of ZnO according to ICDD 01-079-9878.

The quality of the orientation of the ZnO coatings was calculated using the diffractograms of Fig. 1 and the relative texture coefficient (T<sub>c</sub>) [15]. This calculation is a related measure of the degree of preferential orientation shown by the material during growth in the hydrothermal stage, indicating

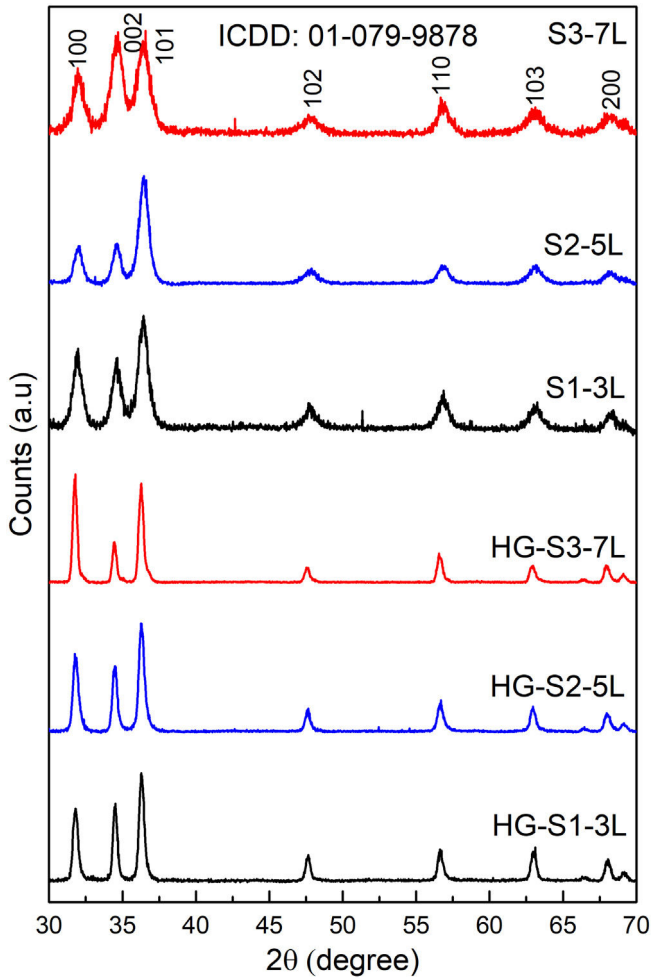


**Fig. 1 – X-ray diffraction patterns of ZnO seed layer (S1-3L, S2-5L and S3-7L) and hydrothermal growth (HG-S1-3L, HG-S2-5L and HG-S3-7L).**

the plane in which the material has a preference to grow under the conditions of synthesis of this work (2):

$$TC_{hkl} = \frac{(I_{hkl}/I_{hkl}^0)}{(\sum_N(I_{hkl}/I_{hkl}^0))} \quad (2)$$

where  $TC_{(hkl)}$  is the diffraction relating coefficient peaks corresponding to the interested plane. The term  $I_{hkl}^0$  is the standard diffraction intensity according to the ICDD crystallographic chart 01-079-9878, measurements from an oriented powder sample random.  $\sum_N$  is the sum of the Bragg reflection number included in the analysis. Finally,  $I_{hkl}$  is the diffraction intensity measured from the plane of interest of the material characterized.

The calculated values of  $T_c$  of the planes (100), (002), and (101) of the coatings are shown in Fig. 2. It observed that the  $T_c$  values for the HG-S1-3L and HG-S2-5L overlays are larger in direction (002), so it concludes that nanostructures prefer to grow in this direction compared to other nanostructures

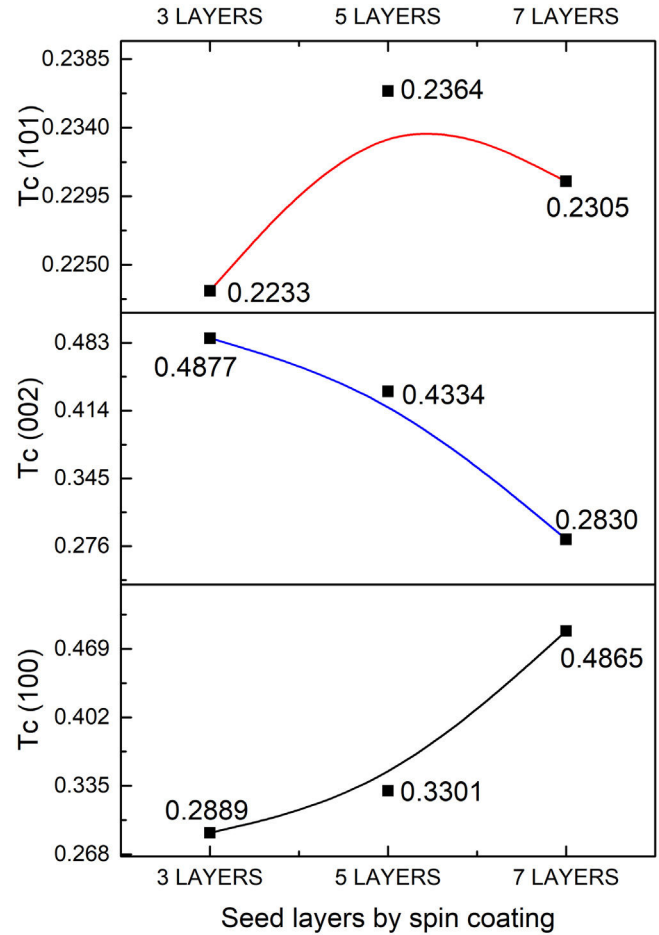


**Fig. 2 – Texture coefficient for hydrothermal growth of ZnO seed layers.**

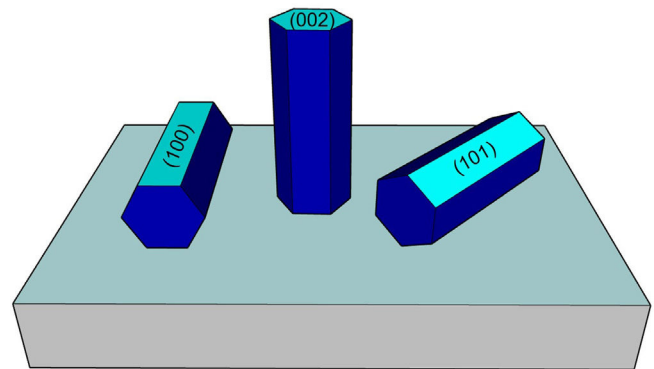


**Fig. 3 – Schematic diagram of the planes in the growth of a hexagonal structure.**

planes, as seen in Fig. 3. In addition, we can also observe that for HG-S3-7L, the values of coefficient  $T_c$ , increased in the direction (100) and (101), but they reduce in address (002). This behavior in the value of  $T_c$  could correspond to the contribution of intensities in the signal due to the presence of flower-shaped structures [16].

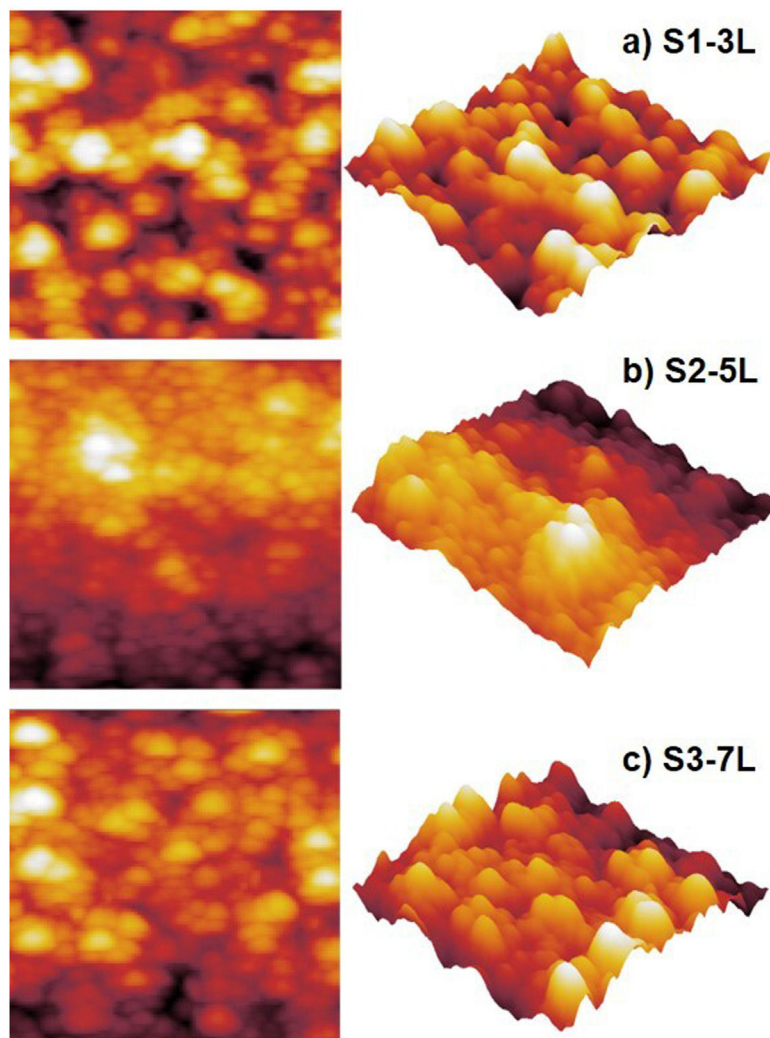


Fig. 4 – AFM image of ZnO seed layer (a) S1-3L, (b) S2-5L and (c) S3-7L.

**Table 1 – Results of the root mean square roughness of ZnO coatings,  $n = 3$ .**

Sample	RMS (nm)
S1-3L	$5 \pm 0.1$
S2-5L	$5 \pm 0.2$
S3-7L	$5 \pm 0.3$

#### Surface morphology of ZnO coatings

Fig. 4 shows the images of the superficial morphology of the samples in a scanned area of  $1.0 \mu\text{m} \times 1.0 \mu\text{m}$ . It is known that the surface roughness of the ZnO coating can be affected by factors such as the shape of the nanostructures, the coating deposition conditions, the heat treatment of the samples, and the chemical reactions in the precursor solutions [17]. Due to the study variables in this work, we consider that the surface roughness of ZnO coatings is due to a coalescence effect in the structures due to spin coating process, and a mechanism of the interpenetration of new layers into the already deposited and heat treated ones [18]. Table 1 shows the roughness results from the root mean square (RMS). These results agree with

the SEM micrographs of the ZnO SL. The cross-sectional surfaces of the ZnO thickness SL were examined by SEM. Fig. 5 shows the process of deposition using the SCT followed by the heat treatment.

According to the profiles of the micrographs of Fig. 6, the thicknesses of the ZnO SL of samples S1-3L, S2-5L, and S3-7L measured by the cross-section they are  $170 \pm 6 \text{ nm}$ ,  $252 \pm 30 \text{ nm}$ , and  $375 \pm 13 \text{ nm}$  respectively. Many authors have mentioned that the increase in the thickness of the seed layer is related to the number of layers, that is, there is a correlation between the number of layers and the thickness [19–21]. Another factor that depends on the number of layers is the density of the seeds on the substrate [22–24]. Therefore, a greater thickness provides a greater growth area, which causes the increase in the diameter and density of ZnO nanorods. However, it has been reported that the length of the ZnO nanorods decreases as the thickness of the seed coat increases [25]. In this same sense, Fig. 7 shows the SEM micrographs of the ZnO coatings deposited by SCT. The surface morphology of the ZnO coatings of the three SL systems (S1-3L, S2-5L and S3-7L) corresponds to the micrographs in Fig. 7a–c. In them, homogeneous coatings with a spherical granular structure

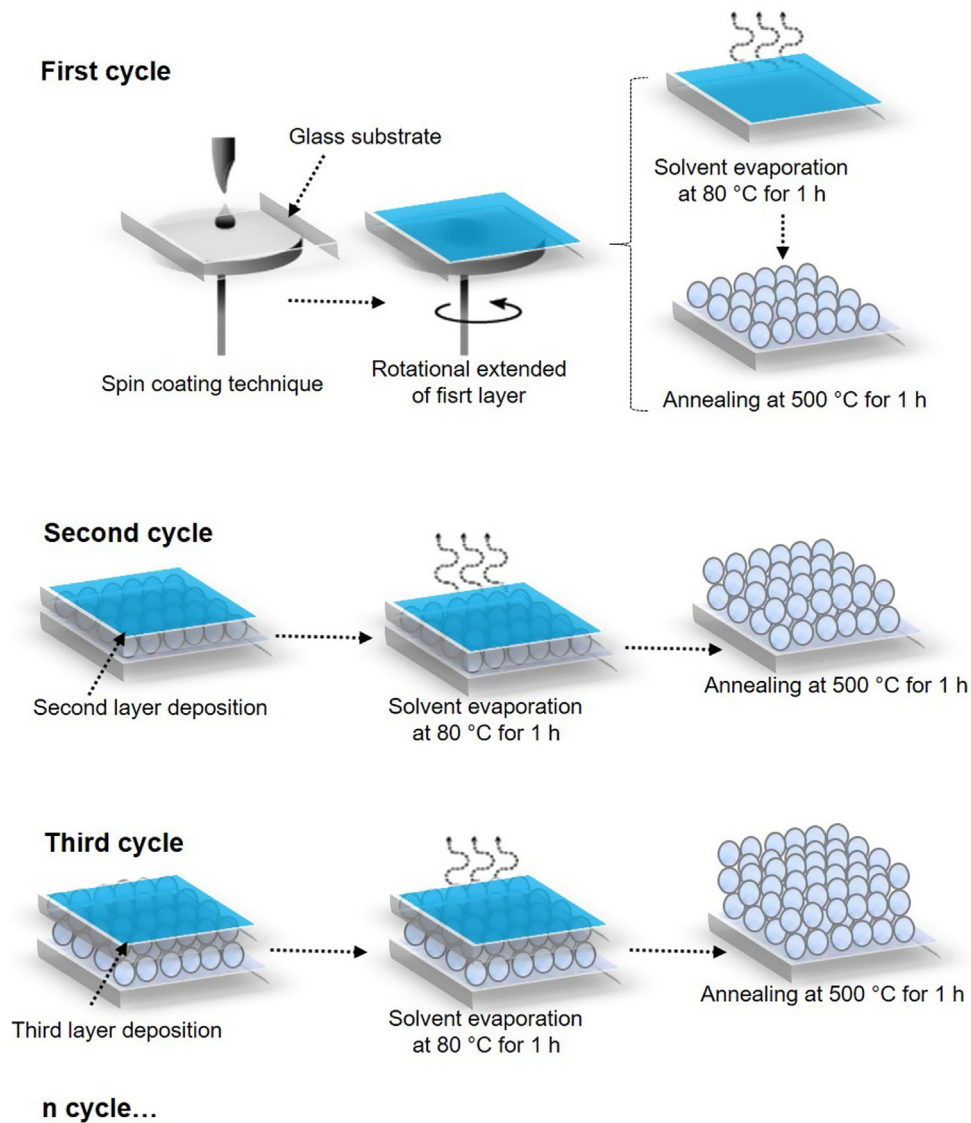


Fig. 5 – Preparation of ZnO coatings.

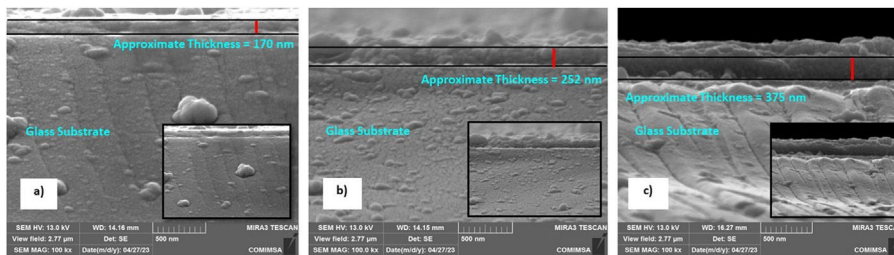


Fig. 6 – SEM cross section view of the seed layers. (a) S1-3L, (b) S2-5L and (c) S3-7L.

are observed whose grain size is  $192 \pm 2$  nm,  $308 \pm 3$  nm and  $231 \pm 5$  nm for S1-3L, S2-5L and S3-7L, respectively. According to the upper and lower surface micrographs of Fig. 8a–c, for the three systems (HG-S1-3L, HG-S2-5L and HG-S3-7L) of hydrothermal growth (HG), the SL with a granular structure resulted in the formation of high-density ZnO nanowires, hexagonal in shape and nanometric sizes (Table 2). Reports

show that the growth of 1D structures is due, as mentioned above, to thickness which in turn influences the density and granular structure of the ZnO SL, which are introduced as nucleation centers and as a controllable alignment agent of ZnO nanorods [26,27].

For the HG-S3-7L (8c) system, in addition to the growth of nanorods, 3D nanostructures in the form of ZnO microflowers

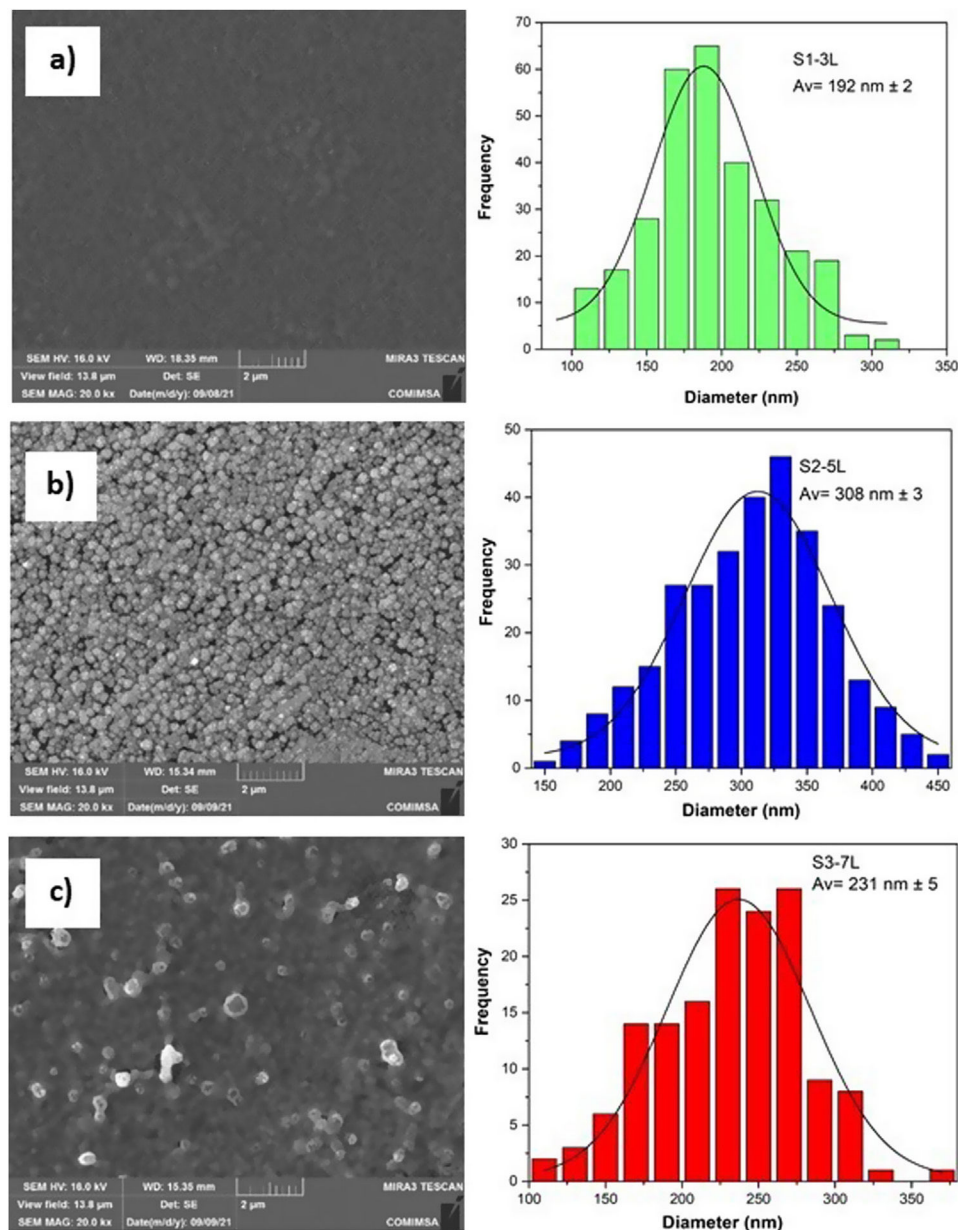


Fig. 7 – SEM of ZnO coatings. Seed layers mean diameters: (a) S1-3L, (b) S2-5L and (c) S3-7L,  $n = 300$ ; view field:  $13.8 \mu\text{m}$ .

Table 2 – Dimensions of ZnO nanostructures with hydrothermal growth.

Sample	Nanorods			
	High surface <sup>a</sup>		Low surface <sup>b</sup>	
	Large (nm)	Diameter (nm)	Large (nm)	Diameter (nm)
HG-S1-3L	$5670 \pm 33$	$1540 \pm 17$	$1538 \pm 55$	$108 \pm 27$
HG-S2-5L	$11,023 \pm 109$	$2352 \pm 23$	$493 \pm 10$	$70 \pm 10$
HG-S3-7L	$7293 \pm 58$	$1518 \pm 19$	$805 \pm 25$	$100 \pm 16$

<sup>a</sup> 300 nanorods at  $50 \mu\text{m}$  resolution.

<sup>b</sup> 100 nanorods at  $1 \mu\text{m}$  resolution.

up to  $6 \mu\text{m}$  in diameter, with petals  $456 \text{ nm}$  wide and  $3 \mu\text{m}$  long, were also obtained. According to Fan et al., the growth process of ZnO nanoflowers is due to the precipitation of  $\text{Zn}(\text{OH})_2$  produced by the combination of  $\text{Zn}^{2+}$  and  $\text{OH}^-$  ions in the solution.

$\text{Zn}(\text{OH})_2$  ions are formed when  $\text{Zn}(\text{OH})_4^{2-}$  is dissolved in water, so it is assumed that the ZnO nanoflowers developed due to an excess concentration of  $\text{Zn}(\text{OH})_4^{2-}$  ions [28], which, in our case, could have occurred by increasing the concentration of avail-

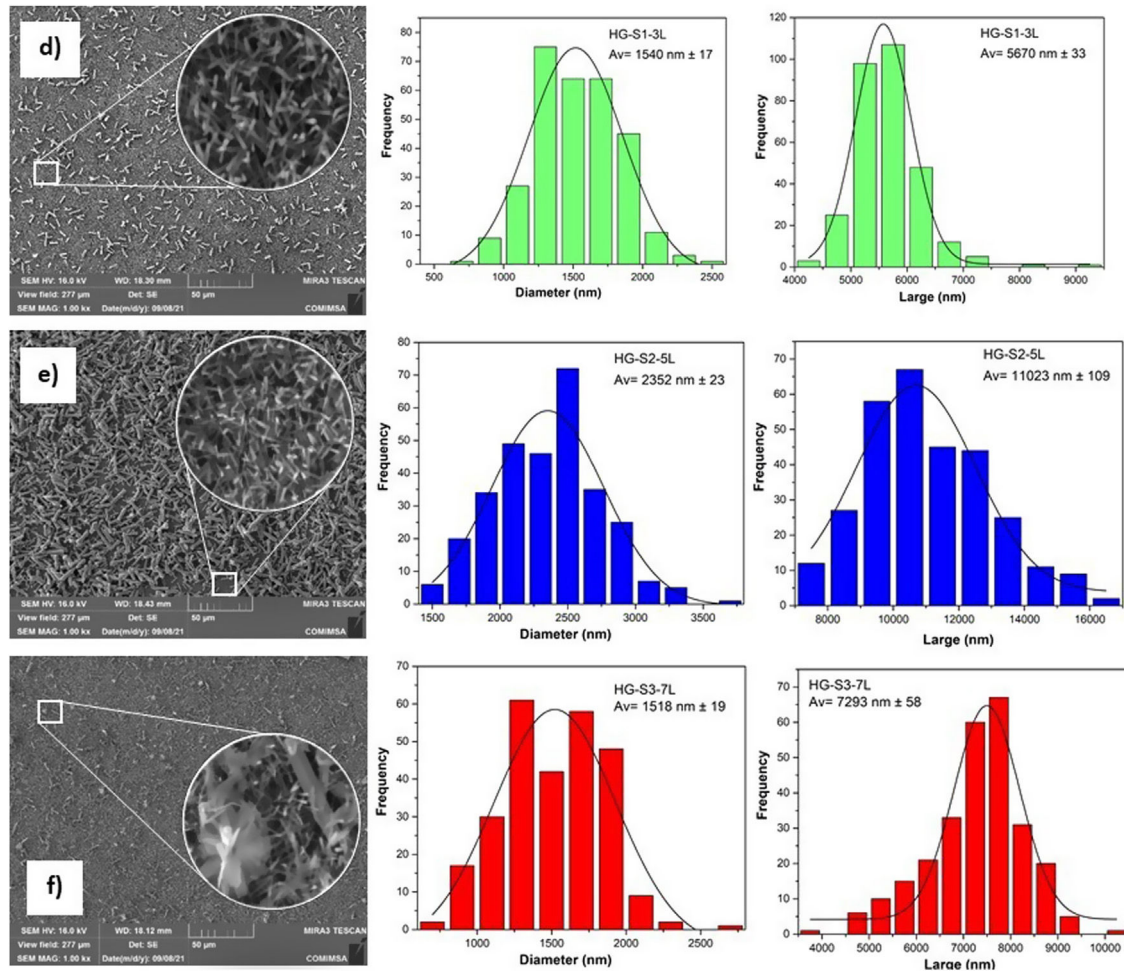


Fig. 8 – SEM of ZnO hydrothermal growth: (a) HG-S1-3L, (b) HG-S2-5L and (c) HG-S3-7L,  $n = 300$ ; view field: 277  $\mu\text{m}$ .

able ions when depositing 7 layers in the S3-7L system. Table 2 shows the average dimensions of the ZnO nanorods on the upper and lower surfaces. The dimensions obtained from the ZnO nanorods are approximate to the values reported (length: 3.000–900 nm; diameter 250–70 nm) in other studies for their photocatalytic application [29,30], in which they used different deposition techniques than those used in this work.

#### Calculation of the hydrothermal growth band gap

ZnO coatings with HG were characterized by UV-Vis diffuse reflectance spectroscopy (DRS) measurements made at room temperature in the 200–400 nm wavelength range and presented in Fig. 9. It is observed that in UV light around 360–370 nm, ZnO coatings are activated. For bandgap energy calculations, reflectance spectra were converted using the Kubelka–Munk (KM) function as an ideal model to relate reflectance and absorbance [31,32] according to Eq. (3).

$$F(R) = \frac{(1 - R)^2}{2R} \quad (3)$$

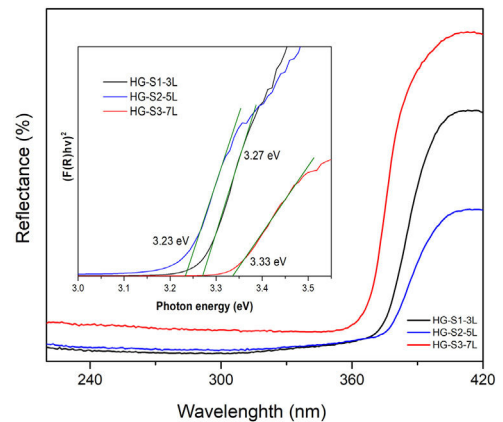
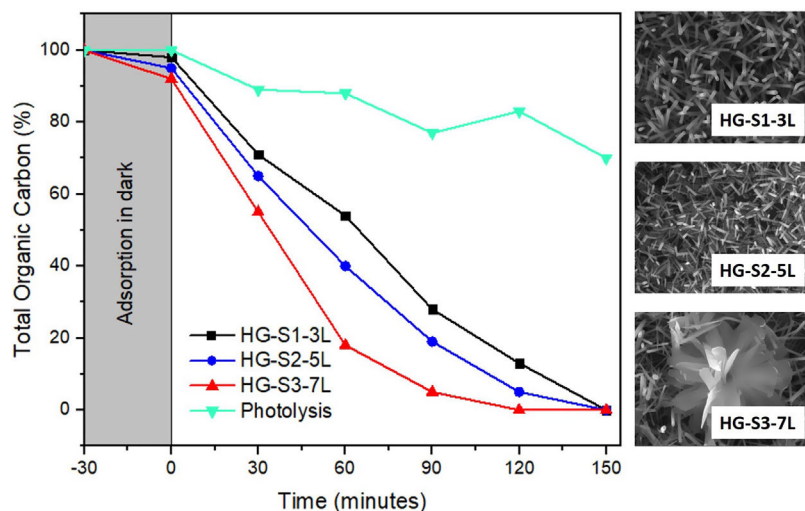


Fig. 9 – Diffuse reflectance of hydrothermal growth of ZnO. With insert graph of the Kubelka–Munk function vs the energy of the photon.

where  $R$  is the reflectance. The use of the KM function makes it possible to obtain graphs analogous to Tauc [33,34], according to Eq. (4).

$$(F(R)hv)^2 = A(hv - E_g) \quad (4)$$



**Fig. 10 – Graph of %TOC vs. irradiation time for the photocatalytic evaluation of methylene blue subjected to degradation with combined ZnO coatings under UV light irradiation.**

In the graph of  $(F(R)hv)^2$  versus photon energy (eV) inserted in Fig. 9, the value of the x-intercept corresponds to the bandgap energy of the coatings with HG. According to the band structure of a semiconductor, the band gap is the difference in energy between the conduction band and the valence band. The reported standard value of the ZnO band gap is 3.37 eV [35]. In this investigation, the measured values of the band gap obtained are 3.27, 3.23, and 3.33 eV, which indicates that they are similar to the values reported in the literature, and no significant changes in the band gap values are reported because our material is pure, in comparison with the values reported in investigations where ZnO is doped with different metals [36–38] or modifications are made in the ZnO synthesis parameters [39,40].

#### Photocatalytic evaluation of ZnO coatings with hydrothermal growth

The photocatalytic activity of the ZnO coatings (HG-S1-3L, HG-S2-5L, or HG-S3-7L), was evaluated for the degradation of  $1 \text{ mgL}^{-1}$  of MB. Using only UV light as a source of activation of the ZnO nanostructures. The TOC analysis of the tests subjected to degradation with the film systems HG-S1-3L, HG-S2-5L, and HG-S3-7L, is shown in Fig. 10. It is observed that the amount of MB degraded during photolysis was 30%. However, with the photocatalytic treatment, it is observed that the best activity has been for HG-S3-7L, reaching a maximum of 100% MB mineralization with irradiation time of 120 min and a rate constant of  $2.98 \times 10^{-2} \text{ min}^{-1}$ . One of the factors that benefit the photocatalytic activity in one-dimensional nanostructures

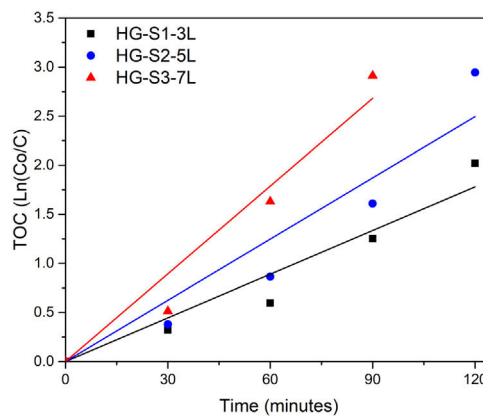


**Fig. 11 – MB reaction kinetics.**

is the length of the nanorods. In them, the photoexcited electrons migrate along the axis of the nanostructure toward the tip of the nanorod, while the holes migrate to the sides, leading to an effective separation of the photogenerated charges [41] responsible for generating the  $\cdot\text{OH}$  that cause the mineralization of the MB. Considering the above, the density of the nanorods on the glass substrate results as another important factor that benefits the photocatalytic efficiency. In our case, according to Fig. 11 and the values in Table 3, the higher density of rods observed in the HG-S3-7L system resulted in a higher rate of dye mineralization. Studies have been done indicating that the polar face (002) promotes a better photocatalytic response because they are more active surfaces

**Table 3 – Kinetics of MB degradation from ZnO thin films with hydrothermal growth.**

	TOC (%) 120 min	Kapp ( $\text{min}^{-1}$ )	$t_{1/2}$ (min)	$R^2$
HG-S1-3L	13	$1.48 \times 10^{-2}$	46.8342	0.9728
HG-S2-5L	5	$2.08 \times 10^{-2}$	33.3243	0.9607
HG-S3-7L	0	$2.98 \times 10^{-2}$	23.2599	0.9805

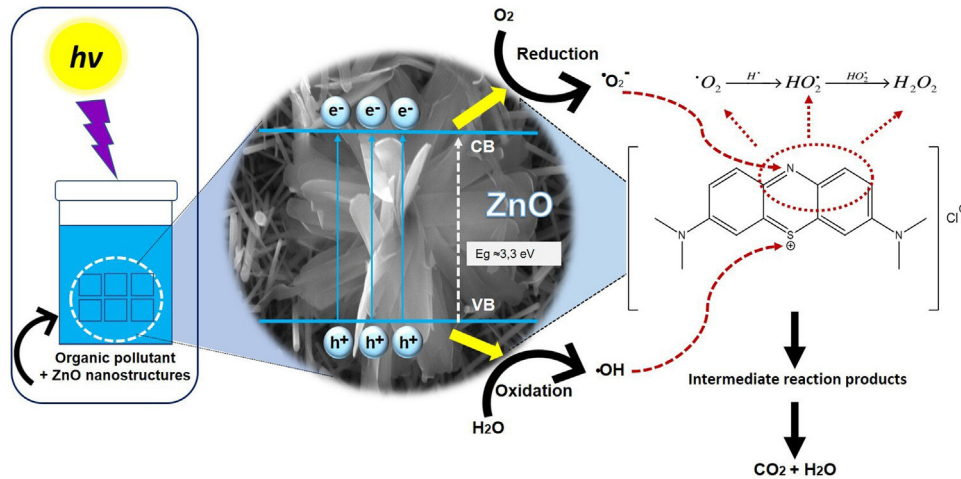


Fig. 12 – Degradation mechanism of MB by ZnO nanostructures.

Table 4 – Results of the photocatalytic degradation of MB with ZnO nanostructures.

ZnO nanostructure	Maximum degradation (%)	Time (min)	Reference
Grains	60	380	[36]
Nanorods assembled flowers	91	140	[37]
Grass	90	150	[38]
Nanorods and microflowers	100	120	Present work

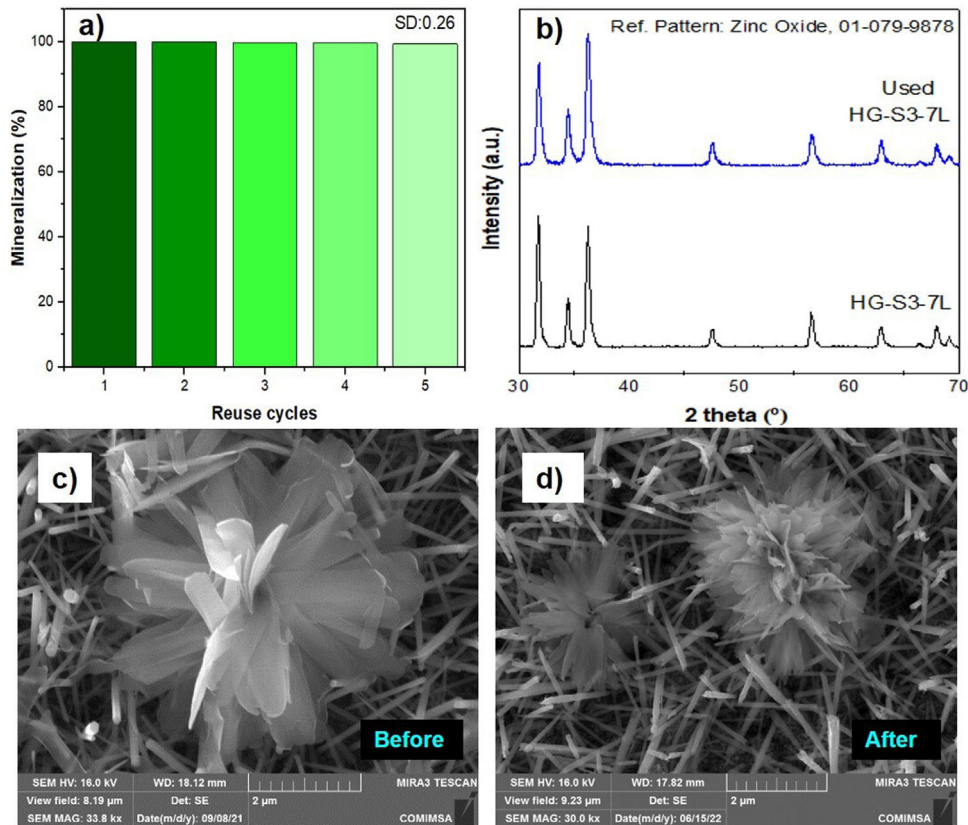


Fig. 13 – (a) Reuse cycles using ZnO, (b) X-ray diffraction, ZnO micrograph (c) before and (d) after the reuse cycles.

compared to the non-polar surfaces (100) and (101) perpendicular to them [42]. In addition to the above, it has been mentioned that nanoflowers provide a large surface area that

allows a long charge transfer that can promote increased photocatalytic efficiency observed in ZnO with this type of 3D nanostructures compared to those with ZnO nanorods. There-

fore, a higher density of 1D nanostructures and a long surface area provided by the 3D nanostructures (see Figs. 8 and 10) results in greater exposure of the polar face of the (002) plane and a long transfer of the photogenerated charges that cause a greater photocatalytic activity in HG-S3-7L.

To know the kinetic parameters of the photocatalytic transformation process of MB, the rate constant ( $k$ ) was calculated using the kinetic equation  $\ln(C/C_0) = -k \cdot t$  (see Table 3). The fit graphs of Fig. 11 indicate that the degradation reaction photocatalytic of MB is of the first order in all treatments.

Fig. 12 shows the possible photocatalytic mechanism of this investigation. First, an absorption equilibrium is set from the liquid phase of the organic pollutant (MB) to the surface of the ZnO after the ZnO is irradiated with UV light with an energy of 4.48 eV. This promotes the excitation of electrons from the valence band (BV) to the conduction band (BC) generating hole pairs of electrons ( $e^-/h^+$ ). These species migrate to the ZnO surface and participate in oxidation and reduction reactions in the adsorbed phase. The holes generated ( $h^+$ ) in the valence band of ZnO react with the molecules of water and hydroxide ions to produce hydroxyl radicals. While electrons ( $e^-$ ) react with oxygen to produce superoxide radical anions and then peroxide hydrogen. The hydrogen peroxide will then react with the superoxide radicals to form hydroxyl radicals. These resulting hydroxyl radicals act as effective oxidants agents to transform the MB adsorbed on the ZnO surface into compound intermediaries so finally achieve the mineralization of transformation products [43].

As previously mentioned, there are no reports of using nanorods or nanoflowers obtained from ZnO SL deposited by the SCT for photocatalytic purposes. However, comparing the results of this research with those reported in the literature (see Table 4), it can be assumed that the ZnO films deposited by SCT followed by HG show higher photocatalytic activity in a reasonable time. This time difference in photocatalytic activity is likely by to the synergistic effect of 1D and 3D structures that takes place in the photocatalytic degradation system when using HG-S3-7L.

A feature of a photocatalyst is its reusability. Fig. 13 shows the percentage results of the performance of the HG-S3-7L film system during five consecutive reuse cycles mineralization efficiency kept the range of 100–99.4%, with a standard deviation of  $\pm 0.26$ . This stability is because the ZnO wurtzite crystal structure (Fig. 13b) and the morphology of the ZnO coatings (Fig. 13c, d) are similar before and after the reuse cycles. It indicates that the 1D and 3D nanostructures obtained in this work have high stability during five reuse cycles for the photocatalytic mineralization of MB under the reaction conditions presented.

## Conclusions

The synthesis conditions of the seed layer (spin coating) have an impact on the final morphology of the nanostructure depending on the number of layers deposited, the greater the number of seed layer deposits, the alignment behavior oriented in the planes is favored (100), (002) and (101). Therefore, the combination of the spin-coating technique to deposit ZnO prepared by sol-gel and then grow up ZnO nanostructures

by the hydrothermal method demonstrates that it is possible to obtain coating on glass substrates with the growing of nano and microstructures in the form of nanorods and ZnO micro flowers.

The best results obtained in the dye degradation were for the HG-S3-7L film system attributed to the synergy obtained between the two morphologies (flowers and rods) that promote electronic migration between ZnO and the dye. Consequently, the morphology of ZnO coatings with hydrothermal growth acts as an efficient photocatalyst in the methylene blue degradation obtaining a 100% degradation in a time of 120 min for the HG-S3-7L system.

## Conflicts of interest

The authors declare no conflict of interest.

## Acknowledgments

Authors thank to UJAT for the facilities, Antonia del Rocío López Gumez acknowledges the scholarship provide by CONACYT. Laura Lorena Díaz Flores thanks Project CB CONACYT 2015 number 256221. We also thank Dr. Juan C. Díaz Guillen Cátedra CONACYT-COMIMSA Saltillo for technical assistance in SEM and XRD measurements.

## REFERENCES

- [1] A. Hernández-Ramírez, I. Medina-Ramírez, *Photocatalytic Semiconductors*, Springer International Publishing, Cham, 2015, <http://dx.doi.org/10.1007/978-3-319-10999-2>.
- [2] S. Duo, Y. Li, Z. Liu, R. Zhong, T. Liu, H. Xu, Preparation of ZnO from 2D nanosheets to diverse 1D nanorods and their structure, surface area, photocurrent, optical and photocatalytic properties by simple hydrothermal synthesis, *J. Alloys Compd.* 695 (2017) 2563–2579, <http://dx.doi.org/10.1016/j.jallcom.2016.11.162>.
- [3] K.N. Abbas, N. Bidin, Morphological driven photocatalytic activity of ZnO nanostructures, *Appl. Surf. Sci.* 394 (2017) 498–508, <http://dx.doi.org/10.1016/j.apsusc.2016.10.080>.
- [4] M.A. Borysiewicz, ZnO as a functional material, a review, *Crystals* 9 (2019), <http://dx.doi.org/10.3390/cryst9100505>.
- [5] C.B. Ong, L.Y. Ng, A.W. Mohammad, A review of ZnO nanoparticles as solar photocatalysts: synthesis, mechanisms and applications, *Renew. Sustain. Energy Rev.* 81 (2018) 536–551, <http://dx.doi.org/10.1016/j.rser.2017.08.020>.
- [6] E. Abdel-Fattah, I.A. Elsayed, T. Fahmy, Substrate temperature and laser fluence effects on properties of ZnO thin films deposited by pulsed laser deposition, *J. Mater. Sci. Mater. Electron.* 29 (2018) 19942–19950, <http://dx.doi.org/10.1007/s10854-018-0124-8>.
- [7] J. Cho, S. Hwang, D.-H. Ko, S. Chung, Transparent ZnO thin-film deposition by spray pyrolysis for high-performance metal-oxide field-effect transistors, *Materials (Basel)* 12 (2019), <http://dx.doi.org/10.3390/ma12203423>.
- [8] M.R. Alfaro Cruz, O. Ceballos-Sanchez, E. Luévano-Hipólito, L.M. Torres-Martínez, ZnO thin films deposited by RF magnetron sputtering: effects of the annealing and atmosphere conditions on the photocatalytic hydrogen production, *Int. J. Hydrogen Energy* 43 (2018) 10301–10310, <http://dx.doi.org/10.1016/j.ijhydene.2018.04.054>.

- [9] A. Galan-Gonzalez, A. Gallant, D.A. Zeze, D. Atkinson, Controlling the growth of single crystal ZnO nanowires by tuning the atomic layer deposition parameters of the ZnO seed layer, *Nanotechnology* 30 (2019) 305602, <http://dx.doi.org/10.1088/1361-6528/ab186a>.
- [10] M.E. Fragalà, A. Di Mauro, D.A. Cristaldi, M. Cantarella, G. Impellizzeri, V. Privitera, ZnO nanorods grown on ultrathin ZnO seed layers: application in water treatment, *J. Photochem. Photobiol. A Chem.* 332 (2017) 497–504, <http://dx.doi.org/10.1016/j.jphotochem.2016.09.032>.
- [11] L. Roza, V. Fauzia, M.Y.A. Rahman, Tailoring the active surface sites of ZnO nanorods on the glass substrate for photocatalytic activity enhancement, *Surf. Interfaces* 15 (2019) 117–124, <http://dx.doi.org/10.1016/j.surfin.2019.02.009>.
- [12] F. Bourfaa, A. Boutelala, M.S. Aida, N. Attaf, Y.S. Ocak, Influence of seed layer surface position on morphology and photocatalysis efficiency of ZnO nanorods and nanoflowers, *J. Nanomater.* 2020 (2020) 4072351, <http://dx.doi.org/10.1155/2020/4072351>.
- [13] D.K. Sharma, S. Shukla, K.K. Sharma, V. Kumar, A review on ZnO: fundamental properties and applications, *Mater. Today Proc.* 49 (2022) 3028–3035, <http://dx.doi.org/10.1016/j.matpr.2020.10.238>.
- [14] Y.K. Park, H.S. Choi, J.-H. Kim, J.-H. Kim, Y.-B. Hahn, High performance field-effect transistors fabricated with laterally grown ZnO nanorods in solution, *Nanotechnology* 22 (2011) 185310, <http://dx.doi.org/10.1088/0957-4484/22/18/185310>.
- [15] S. Farhad, N. Tanvir, M. Bashar, M. Hossain, M. Sultana, N. Khatun, Facile synthesis of oriented zinc oxide seed layer for the hydrothermal growth of zinc oxide nanorods, *Bangladesh J. Sci. Ind. Res.* 53 (2018) 233–244, <http://dx.doi.org/10.3329/bjsir.v53i4.39186>.
- [16] Q.I. Rahman, M. Ahmad, S.K. Misra, M.B. Lohani, Hexagonal ZnO nanorods assembled flowers for photocatalytic dye degradation: growth, structural and optical properties, *Superlatt. Microstruct.* 64 (2013) 495–506, <http://dx.doi.org/10.1016/j.spmi.2013.10.011>.
- [17] T. Amakali, L.S. Daniel, V. Uahengo, N.Y. Dzade, N.H. de Leeuw, Structural and optical properties of ZnO thin films prepared by molecular precursor and sol-gel methods, *Crystals* 10 (2020), <http://dx.doi.org/10.3390/cryst10020132>.
- [18] C. Gumiel, T. Vranken, M.S. Bernardo, T. Jardiel, A. Hardy, M.K. Van Bael, M. Peiteado, Thin film composites in the BiFeO<sub>3</sub>-Bi<sub>4</sub>Ti<sub>3</sub>O<sub>12</sub> system obtained by an aqueous solution-gel deposition methodology, *Bol. La Soc. Español. Cerám. Vidr.* 57 (2018) 19–28, <http://dx.doi.org/10.1016/j.bsevcv.2017.09.001>.
- [19] S.N. Sadikin, M.Y.A. Rahman, A.A. Umar, M.M. Salleh, Effect of spin-coating cycle on the properties of TiO<sub>2</sub> thin film and performance of DSSC, *Int. J. Electrochem. Sci.* 12 (2017) 5529–5538, <http://dx.doi.org/10.20964/2017.06.57>.
- [20] L.W. Ji, S.M. Peng, J.S. Wu, W.S. Shih, C.Z. Wu, I.T. Tang, Effect of seed layer on the growth of well-aligned ZnO nanowires, *J. Phys. Chem. Solids* 70 (2009) 1359–1362, <http://dx.doi.org/10.1016/j.jpcs.2009.07.029>.
- [21] D.C. Kim, B.H. Kong, H.K. Cho, D.J. Park, J.Y. Lee, Effects of buffer layer thickness on growth and properties of ZnO nanorods grown by metalorganic chemical vapour deposition, *Nanotechnology* 18 (2007) 15603, <http://dx.doi.org/10.1088/0957-4484/18/1/015603>.
- [22] X. Li, J. Wang, J. Yang, J. Lang, J. Cao, F. Liu, H. Fan, M. Gao, Y. Jiang, Size-controlled fabrication of ZnO micro/nanorod arrays and their photocatalytic performance, *Mater. Chem. Phys.* 141 (2013) 929–935, <http://dx.doi.org/10.1016/j.matchemphys.2013.06.028>.
- [23] P.K. Giri, S. Dhara, R. Chakraborty, Effect of ZnO seed layer on the catalytic growth of vertically aligned ZnO nanorod arrays, *Mater. Chem. Phys.* 122 (2010) 18–22, <http://dx.doi.org/10.1016/j.matchemphys.2010.02.027>.
- [24] T. Ma, M. Guo, M. Zhang, X. Wang, The effect of the texture and the density of ZnO seed layer on the orientation of ZnO nanorod arrays, *J. Nanosci. Nanotechnol.* 9 (2009) 5920–5926, <http://dx.doi.org/10.1166/jnn.2009.1239>.
- [25] Z.H. Azmi, S.N. Mohd Aris, S. Abubakar, S. Sagadevan, R. Siburian, S. Paiman, Effect of seed layer on the growth of zinc oxide nanowires by chemical bath deposition method, *Coatings* 12 (2022), <http://dx.doi.org/10.3390/coatings12040474>.
- [26] S.-N. Bai, S.-C. Wu, Synthesis of ZnO nanowires by the hydrothermal method, using sol-gel prepared ZnO seed films, *J. Mater. Sci. Mater. Electron.* 22 (2011) 339–344, <http://dx.doi.org/10.1007/s10854-010-0139-2>.
- [27] I. Cesini, M. Kowalczyk, A. Lucantonio, G. D'alesio, P. Kumar, D. Camboni, L. Massari, P. Pingue, A. De Simone, A.F. Morgera, C.M. Oddo, Seedless hydrothermal growth of ZnO nanorods as a promising route for flexible tactile sensors, *Nanomaterials* 10 (2020) 16–18, <http://dx.doi.org/10.3390/nano10050977>.
- [28] J. Fan, T. Li, H. Heng, Hydrothermal growth of ZnO nanoflowers and their photocatalyst application, *Bull. Mater. Sci.* 39 (2016) 19–26, <http://dx.doi.org/10.1007/s12034-015-1145-z>.
- [29] L.R. Toporovska, A.M. Hryzak, B.I. Turko, V.P. Rudyk, V.S. Tsybul'skyi, R.Y. Serkiz, Photocatalytic properties of zinc oxide nanorods grown by different methods, *Opt. Quant. Electron.* 49 (2017) 408, <http://dx.doi.org/10.1007/s11082-017-1254-6>.
- [30] M. Faisal, A.A. Ismail, A.A. Ibrahim, H. Bouzid, S.A. Al-Sayari, Highly efficient photocatalyst based on Ce doped ZnO nanorods: controllable synthesis and enhanced photocatalytic activity, *Chem. Eng. J.* 229 (2013) 225–233, <http://dx.doi.org/10.1016/j.cej.2013.06.004>.
- [31] A. Pignataro Machado, S. Amaral Carminati, E. Ribeiro Januário, P. Silvaino Ferreira, J. Moreira Vaz, E.V. Spinacé, Photocatalytic methane conversion over Pd/ZnO photocatalysts under mild conditions, *Methane* 2 (2023) 44–55, <http://dx.doi.org/10.3390/methane2010003>.
- [32] M. Pal, U. Pal, J.M.G.Y. Jiménez, F. Pérez-Rodríguez, Effects of crystallization and dopant concentration on the emission behavior of TiO<sub>2</sub>:Eu nanophosphors, *Nanoscale Res. Lett.* 7 (2012) 1, <http://dx.doi.org/10.1186/1556-276X-7-1>.
- [33] W. Vallejo, A. Cantillo, B. Salazar, C. Diaz-Urbe, W. Ramos, E. Romero, M. Hurtado, Comparative study of ZnO thin films doped with transition metals (Cu and Co) for methylene blue photodegradation under visible irradiation, *Catalysts* 10 (2020), <http://dx.doi.org/10.3390/catal10050528>.
- [34] B.D. Vezbicke, S. Patel, B.E. Davis, D.P. Birnie III, Evaluation of the Tauc method for optical absorption edge determination: ZnO thin films as a model system, *Phys. Status Solidi.* 252 (2015) 1700–1710, <http://dx.doi.org/10.1002/pssb.201552007>.
- [35] H. Çolak, E. Karaköse, G. Kartopu, Effect of consumption of the sol-gel deposited ZnO seed layer on the growth and properties of high quality ZnO nanorods, *J. Mater. Sci. Mater. Electron.* 29 (2018) 11964–11971, <http://dx.doi.org/10.1007/s10854-018-9298-3>.
- [36] K. Qi, X. Xing, A. Zada, M. Li, Q. Wang, S. Liu, H. Lin, G. Wang, Transition metal doped ZnO nanoparticles with enhanced photocatalytic and antibacterial performances: experimental and DFT studies, *Ceram. Int.* 46 (2020) 1494–1502, <http://dx.doi.org/10.1016/j.ceramint.2019.09.116>.
- [37] M. Chitra, G. Mangamma, K. Uthayarani, N. Neelakandeswari, E.K. Girija, Band gap engineering in ZnO based nanocomposites, *Phys. E Low-Dimens. Syst.*

- Nanostruct. 119 (2020) 113969, <http://dx.doi.org/10.1016/j.physe.2020.113969>.
- [38] G. Mangamma, T.N. Sairam, M. Chitra, M. Manikandan, Tailoring the band gap of ZnO nanostructures using chromium, *Phys. B Condens. Matter.* 610 (2021) 412922, <http://dx.doi.org/10.1016/j.physb.2021.412922>.
- [39] R.C. Rai, M. Guminiak, S. Wilser, B. Cai, M.L. Nakarmi, Elevated temperature dependence of energy band gap of ZnO thin films grown by e-beam deposition, *J. Appl. Phys.* 111 (2012) 73511, <http://dx.doi.org/10.1063/1.3699365>.
- [40] Y. Wang, J. Yang, H. Jia, M. Yu, H. Jin, Self-assembled urchin-like ZnO nanostructures fabricated by electrodeposition–hydrothermal method, *J. Alloys Compd.* 665 (2016) 62–68, <http://dx.doi.org/10.1016/j.jallcom.2016.01.060>.
- [41] V. Tiron, M.A. Ciolan, G. Bulai, G. Mihalache, F.D. Lipsa, R. Jijie, Efficient removal of methylene blue and ciprofloxacin from aqueous solution using flower-like, nanostructured ZnO coating under UV irradiation, *Nanomaterials* 12 (2022), <http://dx.doi.org/10.3390/nano12132193>.
- [42] A. McLaren, T. Valdes-Solis, G. Li, S.C. Tsang, Shape and size effects of ZnO nanocrystals on photocatalytic activity, *J. Am. Chem. Soc.* 131 (2009) 12540–12541, <http://dx.doi.org/10.1021/ja9052703>.
- [43] M.A. Abu-Dalo, S.A. Al-Rosan, B.A. Albiss, Photocatalytic degradation of methylene blue using polymeric membranes based on cellulose acetate impregnated with ZnO nanostructures, *Polymers (Basel)* 13 (2021), <http://dx.doi.org/10.3390/polym13193451>.